Optically tunable bound states in the continuum

Yingyue Boretz,[1] Gonzalo Ordonez,[2] Satoshi Tanaka,[3] and Tomio Petrosky[4,*]

[1]*Center for Studies in Statistical Mechanics and Complex Systems, The University of Texas at Austin, Austin, Texas 78712, USA*

[2]*Department of Physics and Astronomy, Butler University, 4600 Sunset Avenue, Indianapolis, Indiana 46208, USA*

[3]*Department of Physical Science, Osaka Prefecture University, Gakuen-cho 1-1, Sakai 599-8531, Japan*

[4]*Institute of Industrial Science, The University of Tokyo, Tokyo 153-8505, Japan*

(Received 30 October 2013; revised manuscript received 12 March 2014; published 26 August 2014)

We demonstrate the existence of tunable bound states in the continuum (BICs) in a one-dimensional quantum wire with two impurities induced by an intense monochromatic radiation field. We find that there is an interesting type of BIC due to the Fano interference between two optical transition channels, in addition to the ordinary BIC due to geometrical interference between electron wave functions emitted by impurities. In both cases the BIC can be achieved by tuning the frequency of the radiation field. Evidence of the BIC can be obtained by observing the absorption rate of a probe photon.

DOI: 10.1103/PhysRevA.90.023853 PACS number(s): 42.50.Nn, 73.20.Hb, 73.22.Dj, 73.63.Nm

I. INTRODUCTION

The phenomenon of bound states in the continuum (BICs) was first discovered by Wigner and von Neumann [1]. Subsequent studies are found in a number of papers (e.g., [2–11]). Examples of BIC in a double-cavity two-dimensional electron waveguide were reported in [12,13]. An experimental report showed evidence of BICs in superlattice structures of quantum wells with a single impurity site [14]. More recently, electronic BICs were found experimentally in acoustic and optical waveguides [15,16] and quantum well infrared photodetector (QWIP) structures [17].

In general, if a discrete state embeds inside the continuum, the state will become unstable due to the resonance effect. If the transition channels are more than one, the resonance line shape becomes asymmetric due to the quantum interference between those decay channels. The phenomenon is often referred to as Fano interference [18,19]. There are many studies that have followed Fano's work. However, the phenomena of the BICs and the Fano interference have often been studied as individual effects. In this paper we discuss the relation between BICs and Fano interference.

As an example we consider here a tight-binding model with two impurity atoms, as donor and acceptor atoms, attached to a semiconductor nanowire under a constant irradiation of an intense monochromatic radiation field. We shall consider two optical transitions, i.e., intra-atomic and interatomic transitions, which are denoted by T_1 and T_2, respectively, in Fig. 1. In the intra-atomic transition a core-level electron of an impurity is excited by the radiation field into an excited level of the impurity, while in the interatomic transition it is directly excited to the continuous state of the nanowire. These two optical transition channels cause Fano interference.

The main results in this paper are twofold. The first one is a different type of BIC in this system. In this BIC the energy of the bound state depends on the coupling constant g of the interaction between the discrete state and the continuum. This is not the case of an ordinary BIC that has been discussed before (see, e.g., Refs. [6,7]). The ordinary BIC can be found for special values of energy of the discrete state that are imbedded in the continuum, where the energy shift of the discrete state due to the interaction vanishes. This value of the energy may be found by requiring that the so-called self-energy part of the discrete state vanishes. Hence, this type of BIC has the same energy as the unperturbed energy without the interaction. This type of BIC exists in our model.

In addition, however, we found the alternative type of BIC as mentioned above. Since this type of BIC depends on the interaction, we call this a dynamic BIC, while we call the ordinary type of BIC a static BIC. As discussed in [6], the static BIC is due to a geometrical interference in the wire between electron wave functions emitted by impurities.[1] In contrast, the dynamic BIC appears because of the multichannels of the transitions T_1 and T_2, as we will show. Hence, the dynamic BIC is the result of Fano interference.

The second main result is that because of the freedom to choose the frequency of the radiation field, both BICs (the dynamic BIC and static BIC) may exist for a wide range of values of discrete-state energies. This is not the case of the BIC that has been discussed in [6] for the system without the radiation field. Indeed, in the absence of the radiation field, we have shown in [6] that the BIC may exist only for a special value of the discrete energy. In contrast, here one can tune the frequency of the radiation field in order to achieve the BIC for an arbitrary value of the energy of the discrete state. This tunability makes the BIC phenomena much more feasible to observe experimentally.

This paper is organized as follows. In Sec. II we introduce the model. Then we decompose the Hamiltonian of the system into the symmetric part and antisymmetric part so that we can analyze our problem in a much simpler form. In Sec. III we construct the complex eigenvalue of resonance states to analyze the instability of the discrete states inside

[*]Permanent address: Center for Studies in Statistical Mechanics and Complex Systems, The University of Texas at Austin, Austin, Texas 78712, USA.

[1]In other systems such as the system of Ref. [5], the energy of the BIC due to geometrical interference does depend on the interaction; however, in the present system this energy is independent of the interaction. Due to this feature it is much easier to distinguish the two types of BICs in the present system.

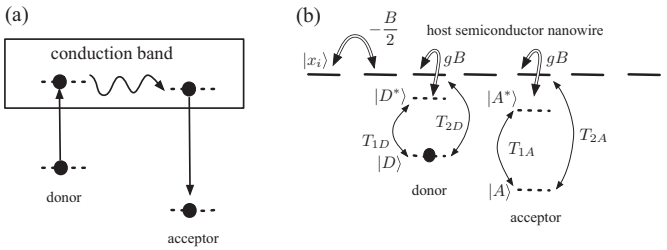

FIG. 1. (a) Energy levels of donor and acceptor atoms. (b) Transitions among energy levels.

the continuum. Then we find the BIC by requiring that the imaginary part of the complex eigenvalue of the Hamiltonian vanishes at the BIC. In Sec. IV we present several cases of the dynamic BIC and the static BIC by plotting the imaginary part of the eigenvalue as a function of the frequency of the radiation field. In Sec. V we study the absorption spectrum of a probe light field, which can be used to detect the BIC. In Sec. VI we summarize our results.

II. MODEL

We consider a semiconductor nanowire with donor-acceptor impurities, e.g., $3d$ transition-metal impurities [20,21], where the multiplet structures of transition metals appear in the semiconductor band gap [22]. An electron of a donor is excited by an optical transition and is transferred to the acceptor through a semiconductor conduction band and the electron is deexcited by an intra-atomic transition to emit a photon (see Fig. 1).

We show the model system of the present work in Fig. 1. The system consists of a semiconductor nanowire with donor and acceptor impurities located at x_D and x_A, respectively. The semiconductor nanowire is described by a one-dimensional (1D) tight-binding model with a nearest-neighbor interaction $-B/2$ yielding a 1D conduction band with bandwidth B with a lattice constant of d. We consider the lower-energy core level and higher-energy excited level of the donor (acceptor) impurity represented by $|D\rangle$ ($|A\rangle$) and $|D^*\rangle$ ($|A^*\rangle$), respectively. In this paper we use the conventional notation of an asterisk to denote excited states used in atomic molecular and optical physics. We consider the charge transfer between the higher-energy state to the nanowire at the impurity sites of x_D and x_A with a coupling gB, where g is a dimensionless coupling constant. The electronic Hamiltonian is then represented by

$$\begin{aligned} H_{el} &= E_D|D\rangle\langle D| + E_{D^*}|D^*\rangle\langle D^*| \\ &\quad + E_A|A\rangle\langle A| + E_{A^*}|A^*\langle A^*| \\ &\quad + E_0\sum_{i=-N/2}^{N/2}|x_i\rangle\langle x_i| - \frac{B}{2}\sum_{\langle i,i'\rangle}|x_i\rangle\langle x_{i'}| \\ &\quad + gB(|x_D\rangle\langle D^*| + |D^*\rangle\langle x_D|) \\ &\quad + gB(|x_A\rangle\langle A^*| + |A^*\rangle\langle x_A|), \end{aligned} \tag{1}$$

where E_D (E_A) and E_{D^*} (E_{A^*}) are the energies of $|D\rangle$ ($|A\rangle$) and $|D^*\rangle$ ($|A^*\rangle$), respectively. The symbol $\langle i,i'\rangle$ represents the sum over nearest neighbors, where the sum runs from $-N$ to N.

The 1D tight-binding Hamiltonian is diagonalized by the wave-number representation defined by

$$|k\rangle = \frac{1}{\sqrt{L}}\sum_{i=-N/2}^{N/2} e^{ikx_i}|x_i\rangle, \tag{2}$$

where under the periodic boundary condition the wave number takes the values of

$$k_j = \frac{2\pi j}{Nd} \tag{3}$$

(where j is an integer $-\frac{N}{2} \leqslant j < \frac{N}{2}$) with the length of the nanowire $L \equiv Nd$. We consider the case $N \gg 1$ and approximate it by taking the limit $N \to \infty$. In this limit we have

$$\frac{2\pi}{L}\sum_{j=-N/2}^{N/2} \to \int_{-\pi/d}^{\pi/d} dk, \quad \frac{2\pi}{L}\delta^{Kr}_{j,j'} \to \delta(k-k'), \tag{4}$$

where δ^{Kr} stands for Kronecker delta. We will take this limit in Sec. III.

In terms of the wave-number representation, H_{el} reads

$$\begin{aligned} H_{el} &= E_D|D\rangle\langle D| + E_{D^*}|D^*\rangle\langle D^*| \\ &\quad + E_A|A\rangle\langle A| + E_{A^*}|A^*\rangle\langle A^*| \\ &\quad + \sum_{k=-\pi/d}^{\pi/d} E_k|k\rangle\langle k| \\ &\quad + \frac{gB}{\sqrt{L}}\sum_{k=-\pi/d}^{\pi/d}(e^{-ikx_D}|k\rangle\langle D^*| + e^{ikx_D}|D^*\rangle\langle k|) \\ &\quad + \frac{gB}{\sqrt{L}}\sum_{k=-\pi/d}^{\pi/d}(e^{-ikx_A}|k\rangle\langle A^*| + e^{ikx_A}|A^*\rangle\langle k|), \end{aligned} \tag{5}$$

where the dispersion relation of an electron in the continuum is given by

$$E_k = E_0 - B\cos(kd). \tag{6}$$

In Eq. (5) and hereafter we use the summation notation over wave vector k. The constant E_0 will be set as $E_0 = n\Omega$ due to the presence of an external monochromatic radiation field, discussed next.

The external field has a frequency Ω that is close to the transition energies of $E_{D^*} - E_D$ or $E_{A^*} - E_A$. The radiation field is described by

$$H_R = \hbar\Omega b^\dagger b, \tag{7}$$

where b ($b^\dagger$) is an annihilation (creation) operator for the radiation field. We will denote the number of photons of the radiation field by n.

As for the interaction of the electron with the radiation field, we consider two optical transition paths from the impurity lower levels. One is the intra-atomic transition in which an electron is excited from the lower impurity level to the upper impurity level. The other is the interatomic transition in which an electron at the lower impurity level is directly excited into the host semiconductor nanowire at the impurity site.

Then the interaction Hamiltonian is described under the dipole approximation [3] as

$$\begin{aligned} H_V = {} & T_{1D}(|D^*\rangle\langle D|b + |D\rangle\langle D^*|b^\dagger) \\ & + T_{1A}(|A^*\rangle\langle A|b + |A\rangle\langle A^*|b^\dagger) \\ & + T_{2D}(|x_D\rangle\langle D|b + |D\rangle\langle x_D|b^\dagger) \\ & + T_{2A}(|x_A\rangle\langle A|b + |A\rangle\langle x_A|b^\dagger), \end{aligned} \tag{8}$$

where $T_{1\sigma}$ and $T_{2\sigma}$ $(\sigma = D, A)$ represent the transition strengths for the two optical transitions. Since the monochromatic radiation $\hbar\Omega$ is nearly resonant to the transition from the lower level to the upper level or semiconductor conduction band, we have used the rotating-wave approximation in Eq. (8) where we have neglected further excitation from the conduction electron to higher excited states.

Even though the interactions of the electron with the radiation field $T_{1\sigma}$ and $T_{2\sigma}$ are small, when the the radiation field intensity is large with a large value of n, we have to incorporate the radiation field nonperturbatively in terms of the dressed-state concept. We then consider the composite vector space of the electronic states and the radiation field [23]. Let us denote the number state $|n\rangle$ $(n = 0,1,2,\dots)$ as an eigenstate of the radiation field. Then the composite vector basis is comprised of $|\alpha,n\rangle$, where α denotes the electronic states: $\alpha = D$, A, D^*, A^*, and k. In terms of these basis, total Hamiltonian is described by

$$\begin{aligned} H = H_{el} + H_R + H_V = {} & \sum_{n=0}^{\infty} \sum_{\alpha=D,A,D^*,A^*,k} (E_\alpha + \hbar\Omega n)|\alpha,n\rangle\langle\alpha,n| \\ & + \frac{gB}{\sqrt{L}} \sum_{n=0}^{\infty} \sum_{k=-\pi/d}^{\pi/d} (e^{-ikx_D}|k,n\rangle\langle D^*,n| + e^{ikx_D}|D^*,n\rangle\langle k,n| + e^{-ikx_A}|k,n\rangle\langle A^*,n| + e^{ikx_A}|A^*,n\rangle\langle k,n|) \\ & + \sum_{n=1}^{\infty} \sqrt{n}[T_{1D}(|D^*,n-1\rangle\langle D,n| + |D,n\rangle\langle D^*,n-1|) + T_{1A}(|A^*,n-1\rangle\langle A,n| + |A^*,n\rangle\langle A,n-1|)] \\ & + \sum_{n=1}^{\infty} \frac{\sqrt{n}}{\sqrt{L}} \sum_{k=-\pi/d}^{\pi/d} [T_{2D}(e^{-ikx_D}|k,n-1\rangle\langle D,n| + e^{ikx_D}|D,n\rangle\langle k,n-1|) \\ & + T_{2A}(e^{-ikx_A}|k,n-1\rangle\langle A,n| + e^{ikx_A}|A,n\rangle\langle k,n-1|)]. \end{aligned} \tag{9}$$

This can be also written as

$$\begin{aligned} H = \sum_{n=0}^{\infty} \Bigg(& \sum_{\alpha=D,A} [E_\alpha + \hbar\Omega(n+1)]|\alpha,n+1\rangle\langle\alpha,n+1| + \sum_{\alpha=D^*,A^*,k} (E_\alpha + \hbar\Omega n)|\alpha,n\rangle\langle\alpha,n| \\ & + \frac{gB}{\sqrt{L}} \sum_{k=-\pi/d}^{\pi/d} (e^{-ikx_D}|k,n\rangle\langle D^*,n| + e^{ikx_D}|D^*,n\rangle\langle k,n| + e^{-ikx_A}|k,n\rangle\langle A^*,n| + e^{ikx_A}|A^*,n\rangle\langle k,n|) \\ & + \sqrt{n+1}[T_{1D}(|D^*,n\rangle\langle D,n+1| + |D,n+1\rangle\langle D^*,n|) + T_{1A}(|A^*,n\rangle\langle A,n+1| + |A,n+1\rangle\langle A^*,n|)] \\ & + \frac{\sqrt{n+1}}{\sqrt{L}} \sum_{k=-\pi/d}^{\pi/d} [T_{2D}(e^{-ikx_D}|k,n\rangle\langle D,n+1| + e^{ikx_D}|D,n+1\rangle\langle k,n|) \\ & + T_{2A}(e^{-ikx_A}|k,n\rangle\langle A,n+1| + e^{ikx_A}|A,n+1\rangle\langle k,n|)] \Bigg) \equiv \sum_{n=0}^{\infty} H_n. \end{aligned} \tag{10}$$

Note that the total vector subspace is classified into independent manifolds according to the photon number n [23].

In the present work we solve the complex eigenvalue problem of H. For simplicity, we shall consider a symmetric situation where

$$\begin{aligned} & x_D = -x_A, \quad E_l \equiv E_D = E_A, \\ & E_u \equiv E_{D^*} = E_{A^*}, \quad T_i \equiv T_{iA} = T_{iD}, \end{aligned} \tag{11}$$

where l stands for the lower level and u stands for the upper level. In this case, because of the inversion symmetry of the system, we can further decompose the vector space according to the parity. We denote the symmetrized basis as (for symmetric basis)

$$|S_l,n+1\rangle \equiv \frac{1}{\sqrt{2}}(|D,n+1\rangle + |A,n+1\rangle), \tag{12}$$

$$|S_u,n\rangle \equiv \frac{1}{\sqrt{2}}(|D^*,n\rangle + |A^*,n\rangle), \tag{13}$$

$$|S_k,n\rangle \equiv \frac{1}{\sqrt{2}}(|k,n\rangle + |-k,n\rangle) \tag{14}$$

and (for antisymmetric basis)

$$|P_l,n+1\rangle \equiv \frac{1}{\sqrt{2}}(|D,n+1\rangle - |A,n+1\rangle), \tag{15}$$

$$|P_u,n\rangle \equiv \frac{1}{\sqrt{2}}(|D^*,n\rangle - |A^*,n\rangle), \tag{16}$$

$$|P_k,n\rangle \equiv \frac{1}{\sqrt{2}}(|k,n\rangle - |-k,n\rangle). \tag{17}$$

With these basis, H_n is divided as

$$H_n = H_n^p + H_n^s, \tag{18}$$

where

$$\begin{aligned} H_n^s &= [E_l + \hbar\Omega(n+1)]|S_l,n+1\rangle\langle S_l,n+1| \\ &+ (E_u + n\Omega)|S_u,n\rangle\langle S_u,n| + \sum_{k=-\pi/d}^{\pi/d} E_k|S_k,n\rangle\langle S_k,n| \\ &+ \frac{gB}{\sqrt{L}}\sum_{k=0}^{\pi/d} 2\cos(kx_D)(|S_k,n\rangle\langle S_u,n| + |S_u,n\rangle\langle S_k,n|) \\ &+ T_1\sqrt{n+1}(|S_u,n\rangle\langle S_l,n+1| + |S_l,n+1\rangle\langle S_u,n|) \\ &+ T_2\frac{\sqrt{n+1}}{\sqrt{L}}\sum_{k=0}^{\pi/d} 2\cos(kx_D)(|S_k,n\rangle\langle S_l,n+1| \\ &+ |S_l,n+1\rangle\langle S_k,n|) \end{aligned} \tag{19}$$

and

$$\begin{aligned} H_n^p &= [E_l + \hbar\Omega(n+1)]|P_l,n+1\rangle\langle P_l,n+1| \\ &+ (E_u + n\Omega)|P_u,n\rangle\langle P_u,n| + \sum_{k=-\pi/d}^{\pi/d} E_k|P_k,n\rangle\langle P_k,n| \\ &- \frac{gB}{\sqrt{L}}\sum_{k=0}^{\pi/d} 2i\sin(kx_D)(|P_k,n\rangle\langle P_u,n| - |P_u,n\rangle\langle P_k,n|) \\ &+ T_1\sqrt{n+1}(|P_u,n\rangle\langle P_l,n+1| + |P_l,n+1\rangle\langle P_u,n|) \\ &- T_2\frac{\sqrt{n+1}}{\sqrt{L}}\sum_{k=0}^{\pi/d} 2i\sin(kx_D)(|P_k,n\rangle\langle P_l,n+1| \\ &- |P_l,n+1\rangle\langle P_k,n|). \end{aligned} \tag{20}$$

Hereafter we use the units $d = 1$ and $\hbar = 1$. By taking the limit $L \equiv Nd \to \infty$, summation over the wave number k turns into the integration as in Eq. (4).

III. OPTICAL DRESSED BOUND STATE IN THE CONTINUUM

As we pointed out previously, our main focus is to study the decay process under influence of a constant irradiation of an intense monochromatic optical field. For this purpose, we solve the complex eigenvalue problem of the Hamiltonian [24–26]. The solutions corresponding to unstable state are found on the second Riemann sheet of the complex energy plane. The imaginary part gives decay rate of the unstable state.

We shall solve the complex eigenvalue problem of the Hamiltonian

$$H_n\psi_E = E\psi_E. \tag{21}$$

We start with the antisymmetric sector, i.e., p sector in Eq. (20). We denote the components of the eigenstates in the p sector by

$$\begin{pmatrix} \tilde{D} \\ \tilde{D}^* \\ \tilde{x}_k \end{pmatrix} \equiv \begin{pmatrix} \langle P_l,n+1|\psi_E\rangle \\ \langle P_u,n|\psi_E\rangle \\ \langle P_k,n|\psi_E\rangle \end{pmatrix}. \tag{22}$$

From Eq. (21) we obtain the system of equations (for $d = 1$)

$$\begin{aligned} [E_l + (n+1)\Omega]\tilde{D} + \sqrt{n+1}T_1\tilde{D}^* + \frac{\sqrt{n+1}T_2}{\pi}\int_{-\pi}^{\pi} dk\, i\sin(x_Dk)\tilde{x}_k &= E\tilde{D}, \\ \sqrt{n+1}T_1\tilde{D} + (E_u + n\Omega)\tilde{D}^* + \frac{gB}{\pi}\int_{-\pi}^{\pi} dk\, i\sin(x_Dk)\tilde{x}_k &= E\tilde{D}^*, \\ -\frac{\sqrt{n+1}T_2}{\pi}i\sin(x_Dk')\tilde{D} - \frac{gB}{\pi}i\sin(x_Dk')\tilde{D}^* + \frac{1}{\pi}\int_{-\pi}^{\pi} dk\, E_k\delta(k-k')\tilde{x}_k &= E\tilde{x}_{k'}. \end{aligned} \tag{23}$$

From the above relations we obtain the eigenvalue equation for p sector. With similar calculations, we can also obtain the eigenvalue equations for the symmetric sector, the s sector in Eq. (19). We summarize both p and s sectors into one form as the following eigenvalue equations whose solutions give the resonant-state pole of the resolvent operator $[z - H_n]^{-1}$ at $z = E$ in the second Riemann sheet. The eigenvalue equations are written as

$$\begin{aligned} \beta^{p,s}(z) \equiv{}& [z - (n+1)\Omega - E_l](z - E_u - n\Omega) - (n+1)T_1^2 \\ &- \Xi^{p,s}(z)\left(Bg^2(z - \Omega(n+1) - E_l) + 2g(n+1)T_1T_2 + (n+1)\frac{T_2^2}{B}(z - E_u - n\Omega)\right) = 0, \end{aligned} \tag{24}$$

where $\Xi^{p,s}(z)$ are the self-energies of the Hamiltonian without the lower-energy level and external radiation field, given by [6]

$$\Xi^{p,s}(z) \equiv \frac{1}{\pi}\int_{-\pi}^{\pi} dk\frac{B[1 \pm \cos(2kx_D)]}{z - E_k} = \frac{1}{i\sqrt{1 - \Delta z^2/B^2}}\left[1 \pm \left(-\frac{\Delta z}{B} + i\sqrt{1 - \Delta z^2/B^2}\right)^{2x_D}\right], \tag{25}$$

with the plus and minus for the s and p sectors, respectively, and $\Delta z \equiv z - n\Omega$. Equation (24) is the generalization of Eq. (5) in Ref [6]. Its solutions give poles of Green's functions for the impurities. Setting

$$\Delta z = -B\cos\theta, \tag{26}$$

we have

$$\Xi^{p,s}(z) = \frac{1}{i\sin\theta}(1 \pm e^{i2x_D\theta}). \tag{27}$$

The BIC corresponds to real solution of Eq. (24). Note that if the last term of the equation vanishes, we obtain

$$z = \tfrac{1}{2}\Big\{[(2n+1)\Omega + E_l + E_u] \pm \sqrt{(\Omega + E_l - E_u)^2 + 4(n+1)T_1^2}\Big\}, \tag{28}$$

which are real solutions.

One can show that these are the only real solutions of Eq. (24) as follows. Let us denote the real eigenvalue as

$$z = z_0. \tag{29}$$

Substituting it into Eq. (24), we have

$$\begin{aligned}&\{z_0 - [(n+1)\Omega + E_l]\}[z_0 - (n\Omega + E_u)] - (n+1)T_1^2 \\ &= \Xi^{p,s}(z_0)\Big(\{z_0 - [(n+1)\Omega + E_l]\}Bg^2 + (n+1)2gT_1T_2 \\ &\quad + (n+1)\frac{T_2^2}{B}[z_0 - (E_u + n\Omega)]\Big).\end{aligned} \tag{30}$$

Note that the left-hand side itself and the factor in front of $\Xi^{p,s}(z_0)$ are both real, because all parameters are real. Hence $\Xi^{p,s}(z_0)$ must be real; otherwise, the factor in front must vanish.

Because the BIC energy is within the continuum we must have

$$\left|\frac{z_0 - n\Omega}{B}\right| \leqslant 1. \tag{31}$$

As a result, θ in Eq. (26) is real for $z = z_0$. Therefore, $\Xi^{p,s}(z_0)$ is a complex number with a nonvanishing imaginary part except for

$$\Xi^{p,s}(z) = \frac{1}{i\sin\theta}(1 \pm e^{i2x_D\theta}) = 0. \tag{32}$$

Equation (32) leads to one possible set of BICs that satisfies

$$1 \pm e^{i2x_D\theta} = 0. \tag{33}$$

Then this leads to Eq. (28).

On the other hand, if Eq. (32) is not satisfied, then $\Xi^{p,s}(z)$ is a complex number as mentioned above. Hence, to be consistent with the fact that the left-hand side of Eq. (30) must be real, we have

$$\begin{aligned}&\{z_0 - [(n+1)\Omega + E_l]\}Bg^2 + (n+1)2gT_1T_2 \\ &\quad + (n+1)\frac{T_2^2}{B}[z_0 - (E_u + n\Omega)] = 0.\end{aligned} \tag{34}$$

Hence, once again we obtain Eq. (28). This proves that the z in Eq. (28) are only the real solutions of Eq. (24).

Let us first consider the case of Eq. (32). We notice that the self-energies for the s and p sectors periodically vanish when

$$\theta = \frac{m\pi}{2x_D}\begin{cases}\text{is an even integer } m \text{ for the } p \text{ sector}\\ \text{is an odd integer } m \text{ for the } s \text{ sector}\end{cases} \tag{35}$$

and then the real solution of the eigenvalue equation, i.e., the BIC, is given by

$$z_0 - n\Omega = -B\cos\left(\frac{m\pi}{2x_D}\right). \tag{36}$$

Note that the energies of the BIC are the same as obtained in [6], where z_0 does not depend on g. This is a typical feature of the ordinary BIC in this system, hence the static BIC mentioned in the Introduction comes from a geometrical interference of the two electron wave functions emitted from $|D^*\rangle$ and $|A^*\rangle$ states.

Substituting Eq. (36) into Eq. (30) with the right-hand side equal 0, we obtain an equation for the frequency Ω of the photon that can achieve a static BIC in this system

$$\Omega = \frac{(n+1)T_1^2}{E_u + B\cos\left(\frac{m\pi}{2x_D}\right)} - B\cos\left(\frac{m\pi}{2x_D}\right) - E_l. \tag{37}$$

Note that this frequency does not depend on T_2. Hence, the BIC that appears at this frequency does not come from the Fano interference between the two transition branches corresponding to T_1 and T_2. As discussed in [6], in this BIC the electron is trapped in a delocalized state extended over the two atoms and the section of wire between them.

Next we consider the case of Eq. (34). This case leads to a different type of BIC, which is a main result of the present paper. In contrast to the BIC in Eq. (37), the value of Ω that satisfies Eqs. (34) and (28) must meet the condition

$$\Omega = E_u - E_l - \frac{BgT_1}{T_2} + (n+1)\frac{T_1T_2}{Bg}. \tag{38}$$

It should be noted that the frequency Ω depends on g and T_2, in contrast to the case in Eq. (37).

Hence, we call this BIC the dynamic BIC, as mentioned in the Introduction. Note that in the limit $T_2 \to 0$ the dynamic BIC disappears for $T_1 \neq 0$. Hence, the BIC is a result of the existence of two transition branches associated with T_1 and T_2. In other words, the BIC is a result of Fano interference.

It should be emphasized that all BICs obtained in our system exist for any value of E_u for a suitable value of Ω. This is in contrast to the system without radiation field discussed in [6], where the BICs occur only for special values given by

$$E_u = -B\cos\left(\frac{m\pi}{2x_D}\right). \tag{39}$$

In other words, the BICs in the system with decoupled lower $|D\rangle$ and $|A\rangle$ states occur only for a special kind of intra-atoms with the discrete-state energies given by Eq. (39). In contrast, for the present system in which $T_1 \neq 0$ and $T_2 \neq 0$, the BICs in the system may exist for any intra-atomic levels by tuning the value of Ω. In this sense, it is experimentally more feasible to achieve the BIC in our system than the system we have discussed in [6].

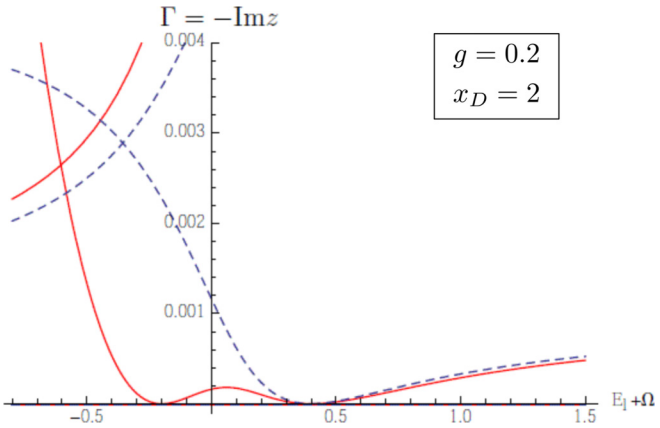

FIG. 2. (Color online) Absolute value of the imaginary part of eigenvalues of the Hamiltonian (p sector) as a function of $\Omega + E_l$. The parameters are $T_1 = 0.2$, $g = 0.2$, $E_u = 0.1$, and $x_D = 2$. Hereafter we use $B/2 = 1$ as the energy unit. The solid line corresponds to $T_2 = 0.2$, while the dashed line corresponds to $T_2 = 0$. The curves on the upper left corner correspond to another solution of Eq. (24). For $T_2 = 0.2$ (solid line) there is a static BIC at $\Omega + E_l = 0.4$ that is independent of the strength of the interaction g. In addition there is a dynamic BIC at $\Omega + E_l = -0.2$ that is due to the interaction with the Fano interference. The $\Omega + E_l$ values for which the BIC occurs in the plot are consistent with Eqs. (37) and (38), respectively. When $T_2 = 0$ (dashed line) the Fano interference is suppressed, so only the first BIC occurs.

IV. BOUND STATES IN THE CONTINUUM AND GENERAL SOLUTION OF THE EIGENVALUE EQUATION (24)

In this section we present numerical results showing the general solution of Eq. (24) as a function of $\Omega + E_l$ and compare them to the analytic solutions of the BIC we obtained in the previous section. For illustration we will consider the simplest case with $n = 0$. The numerical results were obtained through a numerical solution of Eq. (24). In Figs. 2–5 we plot

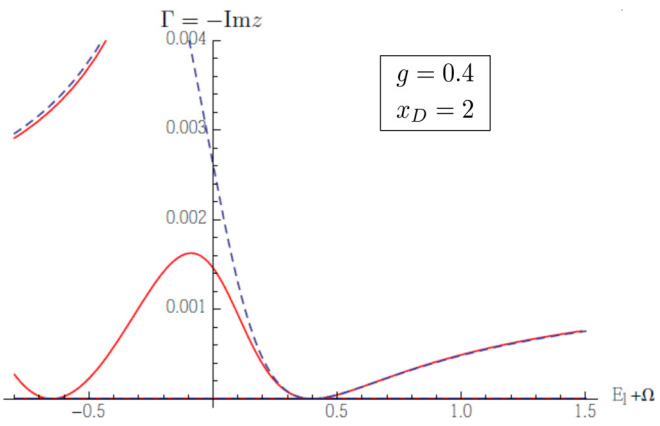

FIG. 3. (Color online) Absolute value of the imaginary part of eigenvalues of the Hamiltonian (p sector) as a function of $\Omega + E_l$. The parameters are the same as in Fig. 2 except for $g = 0.4$. The solid line corresponds to $T_2 = 0.2$, while the dashed line corresponds to $T_2 = 0$. The static BIC that occurs due to the vanishing of the self-energy still occurs at $\Omega + E_l = 0.4$, while the dynamic BIC is shifted to $\Omega + E_l = -0.659$ due to a change of g.

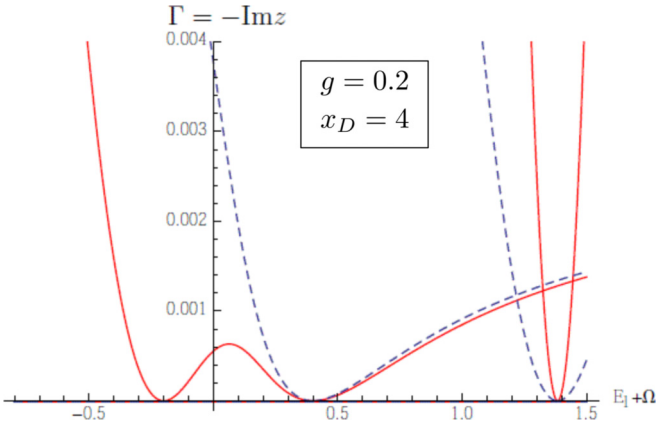

FIG. 4. (Color online) Absolute value of the imaginary part of eigenvalues of the Hamiltonian (p sector) as a function of $\Omega + E_l$. The parameters are the same as in Fig. 2 except for $x_D = 4$. The solid line corresponds to $T_2 = 0.2$, while the dashed line corresponds to $T_2 = 0$. There are two BICs at $\Omega + E_l = 1.38$ and 0.4, where the self-energy vanishes. There is another BIC at $\Omega + E_l = -0.2$, for which the self-energy does not vanish.

the imaginary part of the solution $\Gamma \equiv -\mathrm{Im}z$ as a function of $\Omega + E_l$ for the p sector. The figures for the s sector are essentially the same as those, except the locations of BICs are different.

In Figs. 2–5 we plot the case $E_u = 0.1$ and $T_2 = 0.2$. In all these figures the red solid line corresponds to the case $T_2 = 0.2$ and the blue dashed line corresponds to the case $T_2 = 0$. We consider both cases in order to identify the BIC due to Fano interference.

We show in Fig. 2 the case $x_D = 2$ and $g = 0.2$; in Fig. 3 we have the same $x_D = 2$ but $g = 0.4$. As theoretically predicted, we have two BICs, one from Eq. (37) and the other from Eq. (38) with $\Gamma = 0$.

The BIC at the positive value of $\Omega + E_l$ is the static BIC that exists even in the case $T_2 = 0$. As one can see, the location

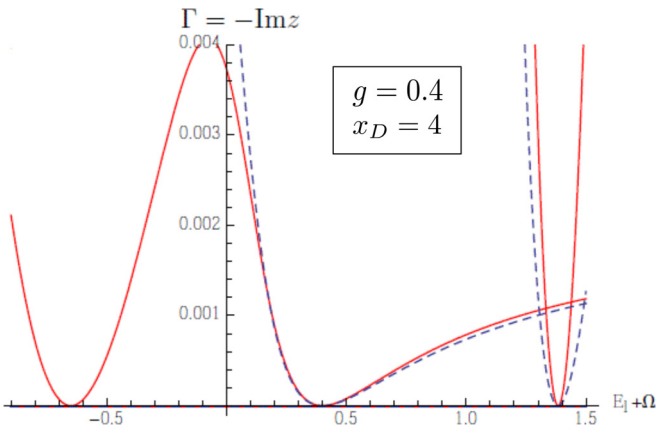

FIG. 5. (Color online) Absolute value of the imaginary part of eigenvalues of the Hamiltonian (p sector) as a function of $\Omega + E_l$. The parameters are the same as in Fig. 4 except for $g = 0.4$. The solid line corresponds to $T_2 = 0.2$, while the dashed line corresponds to $T_2 = 0$. There are two static BICs at $\Omega + E_l = 1.38$ and 0.4, while the dynamic BIC is shifted to $\Omega + E_l = -0.659$ due to a change of g.

of the BIC is at the same point in Figs. 2 and 3, though the value of g is different. The BIC at the negative value of $\Omega + E_l$ in Figs. 2 and 3 is the dynamic BIC that exists only for the case $T_2 \neq 0$. The location of this BIC depends on the value of g (compare Figs. 2 and 3).

We show in Fig. 4 the case $x_D = 4$ and $g = 0.2$; in Fig. 5 we show the case with the same $x_D = 4$ but $g = 0.4$. As predicted, we have different BICs: Two are from Eq. (37) and the other from Eq. (38) with $\Gamma = 0$.

All the static BICs are located at predicted values of $\Omega + E_l$. They exist also in the case $T_2 = 0$. The locations of the static BICs in Fig. 4 appear at the same points in Fig. 5 though the value of g is different. The dynamic BIC appears at the negative values of $\Omega + E_l$ in Fig. 4. We have this dynamic BIC only for $T_2 \neq 0$. The location of the BIC depends on the value g as predicted by Eq. (38).

V. PROBING BOUND STATES IN THE CONTINUUM

Experimental evidence of the BIC can be obtained through the absorption spectrum of the system, which will include sections with a Fano profile [24]. In this section we study the absorption spectrum of a weak probe light field, which could be compared to experimental results.

In our system the radiation field with frequency Ω has to be strong so that it is able to tune the states of the system and produce BICs. Hereafter we will call it the pump field. Since the pump field is strong we need to obtain first the exact eigenstates of the Hamiltonian in order to calculate the absorption spectrum. Subsequently we will add a weak probe field that will be used to detect the BIC.

A. Exact eigenstates of the Hamiltonian

We will obtain the exact scattering eigenstates of the Hamiltonian, which will be the final states after the electron absorbs a probe photon. Solving the system of equations (23), with the condition that the eigenstates reduce to the states $|k\rangle$ when the couplings vanish, we get

$$\tilde{x}_{k'} = \delta(k-k') + \frac{2V_{k'}^*}{E - E_{k'} + i0}(gB\tilde{D}^* + \tilde{T}_2\tilde{D}), \quad (40)$$

$$\tilde{D}^* = \frac{Bg(E - E_l - (n+1)\Omega) + \tilde{T}_1\tilde{T}_2}{\beta(E)}V_k, \quad (41)$$

$$\tilde{D} = \frac{\tilde{T}_2(E - E_u - n\Omega) + \tilde{T}_1 Bg}{\beta(E)}V_k, \quad (42)$$

where k is given by $E = n\Omega - B\cos(k)$, $\tilde{T}_j = \sqrt{n+1}\,T_j$, $V_k = -i\sin(kx_D)$ for the p sector, and $V_k = \cos(kx_D)$ for the s sector. Hereafter we shift the zero of energy so that $E = -B\cos(k)$ (thus effectively we set $n = 0$). We take into account the effect of the intensity of the field n in the renormalized transition strengths $\tilde{T}_j$.

B. Absorption rate

The system described so far includes the pump field with frequency Ω. Now we add a weak probe field, represented by a single photon of frequency ω. We will calculate the absorption rate of the probe photon. The states of the system are shown in

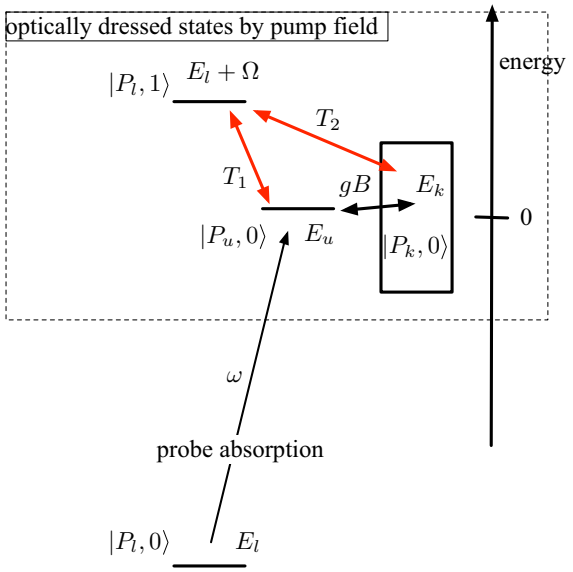

FIG. 6. (Color online) State scheme for pump and probe photons. Depending on the value of Ω the level $E_l + \Omega$ may be below or above the level E_u. The latter case is shown here.

Fig. 6 for the p sector (the diagram for the s sector is identical). As shown in Fig. 6, the lower-level electron in the $|P_l,0\rangle$ state is excited into the $|P_u,0\rangle$ state in the p-sector Hamiltonian by the absorption of the probe photon. The interaction with the weak probe field is given by

$$\hat{U}_p = |P_u,0\rangle U_p \langle P_l,0| + |P_l,0\rangle U_p^* \langle P_u,0|. \quad (43)$$

Similar states and interaction are added to the s-sector Hamiltonian.

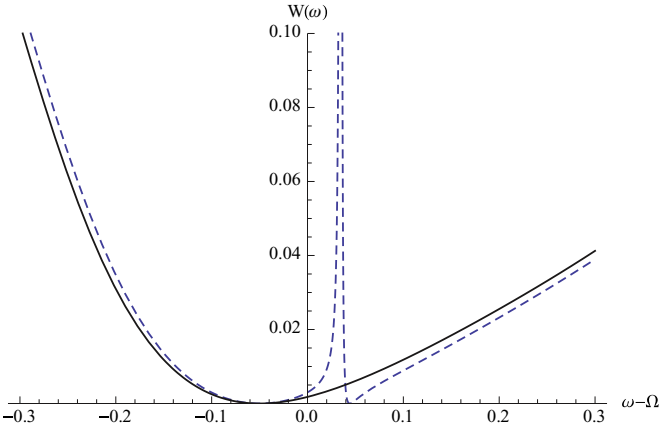

FIG. 7. (Color online) The solid line corresponds to the absorption rate for a pump frequency given by $E_l + \Omega = 1.38$, which allows the existence of a static BIC. The dashed line corresponds to the absorption rate for $E_l + \Omega = 1.37$, slightly off the static BIC value. When the pump frequency is slightly off the static BIC frequency, the absorption rate (dashed line) takes a sharp profile, which in this case occurs near $\omega - \Omega = 0.04$. The sharp profile shape is suppressed when $E_l + \Omega$ is exactly at the BIC value (solid line). For this and the following graph the parameters are $b = 2$, $g = 0.4$, $x_D = 4$, $\tilde{T}_2 = 0.2$, $\tilde{T}_1 = 0.2$, and $E_u = 0.1$. We use units where $\hbar = 1$. The units of frequency and absorption rate are then the same as the energy unit, $B/2 = 1$.

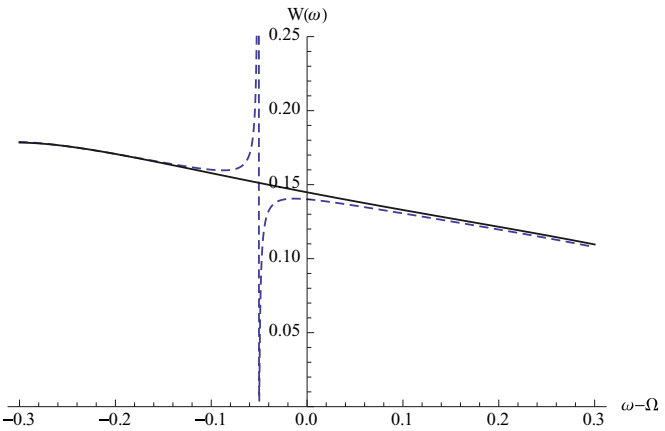

FIG. 8. (Color online) The solid line corresponds to the absorption rate for a pump frequency given by $E_l + \Omega = -0.65$, which allows the existence of a dynamic BIC. The absorption rate shows no sharp shape. The dashed line corresponds to the absorption rate for $E_l + \Omega = -0.64$, slightly off the dynamic BIC value. The absorption rate then takes a sharp shape, which in this case occurs near $\omega - \Omega = -0.5$.

We will calculate the transition rate due to absorption of the probe photon, starting with the initial state $|P_l,0\rangle$ and ending at an eigenstate $|\psi_E\rangle$ of the Hamiltonian. The transition occurs due to the weak interaction $\hat{U}_p$. Similar calculations can be done for the s sector.

Since $\hat{U}_p$ is a weak interaction, we can apply Fermi's golden rule. The final energy of the electron is $E = E_k = -B\cos(k)$. The absorption rate, denoted $W(\omega)$, is then given by

$$\begin{aligned} W(\omega) &= \int_{-\pi}^{\pi} \frac{dk}{2\pi} \left|\langle \psi_{E_k} | \hat{U}_p | P_l,0\rangle\right|^2 2\pi\delta(E_l+\omega-E_k) \\ &= \rho(E_k)\left|\langle \psi_{E_k} | \hat{U}_p | P_l,0\rangle\right|^2_{E_k=E_l+\omega} \\ &= \rho(E_k)|U_p|^2\left|\langle P_u,0|\psi_{E_k}\rangle\right|^2_{E_k=E_l+\omega}, \end{aligned} \tag{44}$$

where $\rho(E) = dk/dE$ is the density of states. Using Eq. (41) we obtain

$$W(\omega) = \rho(E_k)|U_p|^2 \times \left|\frac{Bg(E_k - E_l - \Omega) + \tilde{T}_1\tilde{T}_2}{\beta(E_k)} V_k\right|^2_{E_k=E_l+\omega}. \tag{45}$$

In Figs. 7 and 8 we show the absorption rate as a function of $(E_l+\omega) - (E_l+\Omega) = \omega - \Omega$ for different values of $E_l + \Omega$. When this energy is close (but not exactly equal) to a BIC value, the absorption rate takes a sharp (rapidly varying) profile, which is explained as follows. The equation $\beta(E_k) = 0$ has real solutions $E_k = z_{\rm BIC}$ when Ω approaches specific values $\Omega = \Omega_{\rm BIC}$ given by Eq. (37) or (38). Therefore, when Ω is close to $\Omega_{\rm BIC}$, the factor $1/\beta(E_k)$ in Eq. (45) takes a very large value around $E_k = z_{\rm BIC}$. However, the interaction V_k vanishes when E_k is equal to a static $z_{\rm BIC}$, while the function $\chi(E_k) \equiv Bg(E_k - E_l - \Omega) + \tilde{T}_1\tilde{T}_2$ vanishes when E_k is equal to a dynamic $z_{\rm BIC}$. As a result, the absorption rate changes abruptly from 0 to a very large value when E_k passes through a $z_{\rm BIC}$, producing the sharp profiles. These profiles disappear when Ω is exactly an $\Omega_{\rm BIC}$ because then the zero of $\beta(E_k)$ cancels the zero of either V_k or $\chi(E_k)$.

VI. SUMMARY

In this paper we have considered a tight-binding model of a single electron in a 1D quantum wire with two added impurities. We have shown there are tunable bound states in the continuum, induced by an intense monochromatic radiation field. We found a different type of BIC in this system that we called a dynamic BIC, in addition to the other type of BIC that we called a static BIC. In contrast to the static BIC, the energy of the dynamic BIC depends on the coupling constants g and T_2 between the discrete state of the electron and the continuous state of the electron.

We have shown that the dynamic BIC occurs due to Fano interference between two optical transition paths from the core level to the higher-energy state. Specifically, there is a two-step path involving the T_1 transition followed by the gB transitions and a one-step path involving the T_2 transition only (see Fig. 6). These paths interfere destructively in the energy domain as indicated by Eq. (38). As in Fano's original paper, this interference involves two discrete levels and a continuum; in our case it occurs separately within each of the two impurities; it would occur even if one of the impurities were removed.

On the other hand, the static BIC is due to spatial interference between the two impurities, involving only one-step paths. Even though it involves the energy continuum, this interference is not Fano interference; it would occur even if there were only one transition path for each impurity. The interference occurs between outgoing waves emitted from each impurity. These waves destructively interfere with each other, resulting in an appearance of a bound state confined in between the two impurities. There are two separate interference occurrences: One involves the T_2 transitions for both atoms and another the gB transition for both atoms. Interestingly, the static BIC energies are independent of T_2 and g couplings because the interference occurs in the spatial domain only. However, the location of the static BIC energy (37) depends on the T_1 coupling because the T_1 transition produces a shift in the energy levels of each impurity, which affects the wavelength of the outgoing waves.

Furthermore, we have shown that all BICs obtained in our system are tunable, in the sense that they exist for any value of E_l of the discrete state for a suitable frequency Ω of the radiation field. This is not the case for the ordinary BIC without the radiation field. In this sense, it is experimentally more feasible to achieve the BIC in our system.

Experimental evidence of the BIC can be obtained by observing the absorption of a weak probe field discussed in the present paper.[2] When the frequency of the pump field Ω is tuned close to the value that induces a BIC, the absorption profile shows a sharp profile as shown in Figs. 7 and 8. However, when Ω is exactly at a BIC value, this profile is suppressed.

[2]It may also be of interest to relate our theoretical results, in particular the dynamic BIC, to an experiment that reported BIC in a QWIP [17].

ACKNOWLEDGMENTS

We thank L. E. Reichl, J. Keto, A. Bohm, and S. Garmon for insightful discussions. Y.B. thanks the Robert A. Welch Foundation (Grand No. F-1051) for partial support of this work. G.O. thanks Butler University's Holcomb Awards Committee and the LAS Dean Office for travel support.

[1] J. von Neumann and E. Wigner, Phys. Z. **30**, 465 (1929).
[2] E. C. G. Sudarshan, in *Field Theory, Quantization and Statistical Physics*, edited by E. Tirapegui (Reidel, Dordrecht, 1981), pp. 237–245.
[3] F. H. Stillinger and D. R. Herrick, Phys. Rev. A **11**, 446 (1975).
[4] P. S. Deo and A. M. Jayannavar, Phys. Rev. B **50**, 11629 (1994).
[5] G. Ordonez and S. Kim, Phys. Rev. A **70**, 032702 (2004).
[6] S. Tanaka, S. Garmon, G. Ordonez, and T. Petrosky, Phys. Rev. B **76**, 153308 (2007).
[7] S. Longhi, Eur. Phys. J. B **57**, 45 (2007).
[8] A. F. Sadreev, E. N. Bulgakov, and I. Rotter, Phys. Rev. B **73**, 235342 (2006).
[9] S. Longhi and G. Della Valle, Sci. Rep. **3**, 2219 (2013).
[10] J. M. Zhang, D. Braak, and M. Kollar, Phys. Rev. A **87**, 023613 (2013).
[11] J. M. Zhang, D. Braak, and M. Kollar, Phys. Rev. Lett. **109**, 116405 (2012).
[12] G. Ordonez, K. Na, and S. Kim, Phys. Rev. A **73**, 022113 (2006).
[13] H. Lee and L. E. Reichl, Phys. Rev. B **77**, 205318 (2008).
[14] F. Capasso, C. Sirtori, J. Faist, D. L. Sivco, S.-N. G. Chu, and A. Y. Cho, Nature (London) **358**, 565 (1992).
[15] S. Hein, W. Koch, and L. Nannen, J. Fluid Mech. **692**, 257 (2012).
[16] S. Weimann, Y. Xu, R. Keil, A. E. Miroshnichenko, A. Tunnermann, S. Nolte, A. A. Sukhorukov, A. Szameit, and Y. S. Kivshar, Phys. Rev. Lett. **111**, 240403 (2013).
[17] A. Albo, D. Fekete, and G. Bahir, Phys. Rev. B **85**, 115307 (2012).
[18] U. Fano, II Nuovo Cimento **12**, 154 (1935).
[19] U. Fano, Phys. Rev. **124**, 1866 (1961).
[20] N. Pradhan and D. D. Sarma, J. Phys. Chem. Lett. **2**, 2818 (2011).
[21] P. T. K. Chin, J. W. Stouwdam, and R. A. J. Janssen, Nano Lett. **9**, 745 (2009).
[22] S. Watanabe and H. Kamimura, J. Phys. Soc. Jpn. **56**, 1078 (1987).
[23] C. Cohen-Tannouji, J. Dupont-Roc, and G. Grynberg, *Atom-Photon Interactions* (Wiley InterScience, New York, 1992).
[24] S. Tanaka, S. Garmon, and T. Petrosky, Phys. Rev. B **73**, 115340 (2006).
[25] A. Bohm, *Quantum Mechanics: Foundations and Applications* (Springer, Berlin, 1986).
[26] T. Petrosky, S. Tasaki, and I. Prigogine, Physica A **173**, 175 (1991).